Revisiting Basics of k_La Dependency on Aeration in Bubble Columns: a Is Surprisingly Stable

Moritz Wild[‡], Yannic Mast[‡], and Ralf Takors*

DOI: 10.1002/cite.202200165

This is an open access article under the terms of the Creative Commons Attribution License, which permits use, distribution and reproduction in any medium, provided the original work is properly cited.

Dedicated to Prof. Dr. Christian Wandrey on the occasion of his 80th birthday

A comprehensive experimental characterization of a small-scale bubble column bioreactor (60 mL) is presented. Bubble size distribution (BSD), gas holdup, and k_La were determined for different types of liquids, relevant fermentation conditions and superficial gas velocities u_G. The specific interfacial area a and liquid mass transfer coefficient k_L have been identified independent of each other to unravel their individual impact on k_La. Results show that increasing u_G leads to larger bubbles and higher gas holdup. As both parameters influence a in opposite ways, no increase of a with u_G is found. Furthermore, k_L increases with increasing bubble size outlining that improved oxygen transfer is not the result of higher a but of risen k_L instead. The results build the foundation for further simulative investigations.

Keywords: Antifoam, Bubble column, Bubble size distribution, Fermentation medium, Gas-liquid mass transfer

Received: August 11, 2022; *revised:* December 05, 2022; *accepted:* December 21, 2022

1 Introduction

Microbial fermentation is one of the key approaches in the biotech industry for the sustainable production of commodities, fine chemicals, food and feed additives, biopharmaceuticals and many more. Still the complexity of the processes requires steady research for engineering novel strains and production processes to identify best operational conditions that meet the challenging economic and environmental demands [1]. Commonly, strain and process engineering starts in small-scale to allow parallel testing and to benefit from reduced costs thanks to miniaturization [2].

Currently, related experimental programs are mainly performed in shaking flasks and microtiter plates. Successful research studies already managed to establish highly valuable online monitoring techniques for estimating microbial activities [3], which makes those tools attractive for screening programs. However, given the hydrodynamic characteristics of large-scale bioreactors, miniaturized stirred tanks and bubble column reactors may offer more similarity with the production setting [4]. This may lead to improved physiological resemblance with production scale while offering enough sampling volume even for comprehensive metabolic and transcriptional tests. Regarding simplicity, mini bubble columns possess advantages compared to miniaturized stirred tanks as no moving parts are necessary, designs are rather simple, and necessary power inputs for gaining sufficient mixing and oxygen transfer are relatively low [5]. Hence, small-scale bubble columns may be a promising tool for miniaturized and parallelized strain and process engineering provided that key performance criteria for designs are well understood.

During the last two decades several mini bubble column bioreactors have been proposed [6–8] that were successfully used for microbial cultivation purposes. In general, the performance of a bubble column reactor is influenced by various factors such as bubble size distribution, gas holdup, liquid properties, presence of surfactants and temperature [9]. In this context, the integral volumetric mass transfer coefficient k_La is one of the most important design parameters for aerobic process. However, as a merged parameter, comprising a and k_L, it does not provide detailed insight into underlying mass transfer mechanisms [10]. Furthermore, a comprehensive literature review [9] shows that different media compositions significantly affect bubble diameters and mass transfer. In turn, the observations ask for testing various media compositions to get k_L and a values for a sound mechanistic evaluation. Despite the importance of k_La, only few research studies targeted the separated analysis of a and k_L [11]. Indeed, such studies are challenging as they require the independent measurement of gas holdup ε, of bubble size distributions to estimate the Sauter mean diameter d_{32} [12], and k_La measurements.

[1]Moritz Wild, [1]Yannic Mast, [1]Prof. Dr.-Ing. Ralf Takors (takors@ibvt.uni-stuttgart.de)

[1]University of Stuttgart, Institute of Biochemical Engineering, Allmandring 31, 70569 Stuttgart, Germany.

[‡] Both authors contributed equally to this work.

 © 2023 The Authors. Chemie Ingenieur Technik published by Wiley-VCH GmbH

Consequently, this contribution investigated several media compositions for identifying k_L and a separately. It will be shown why k_La values improve with rising aeration, which will support the optimum design of small-scale bubble columns as a tool for strain and bioprocess engineering.

2 Material and Methods

2.1 k_La Determination

For determination of k_La, the dynamic gassing-out technique was applied. It is based on replacing the oxygen fraction in the liquid phase by, e.g., nitrogen stripping to reach 0 % air saturation (a.s). Subsequent, aeration of the system is started and the increase in dissolved oxygen tension is monitored over time as described in [7]. Gas volume flow was controlled by a thermal mass flow controller (Typ GSC-B3KA-BB23, Vögtlin Instruments GmbH, Muttenz, Switzerland). Dissolved oxygen concentrations were measured every 0.2 s by an optical oxygen probe (OXYBase, WR-RS485-A0-L5, PreSens Precision Sensing GmbH, Regensburg, Germany). The probe response time of 3 s was taken from the manufacturer's manual. Nonlinear regression of a first-order approximation to consider the influence of the probe response time was used for calculating k_La values. The measurement was conducted at 37 °C and atmospheric pressure.

2.2 Media Composition

Four different liquids were used: deionized H_2O, 1 × phosphate buffer solution (PBS), minimal medium and minimal medium containing 0.05 % (V/V) antifoam (AF) (Struktol J647, Schill+Seilacher, Hamburg, Germany). The phosphate buffer solution contained 8 g L^{-1} NaCl, 0.2 g L^{-1} KCl, 1.42 g L^{-1} Na_2HPO_4, and 0.27 g L^{-1} KH_2PO_4. Minimal media based on [13] was prepared as follows: 14.5 g L^{-1} glucose × H_2O, 2.6 g L^{-1} K_2HPO_4, 1 g L^{-1} NaH_2HPO_4, 9 g L^{-1} $(NH_4)_2SO_4$, 20 g L^{-1} MOPS and 2 mL L^{-1} of trace element stock solution. The trace element stock solution contained 55 g L^{-1} $Na_3C_6H_5O_7 \times 2$ H_2O, 4.175 g L^{-1} $FeCl_3 \times 6$ H_2O, 0.045 g L^{-1} $ZnSO_4 \times 7$ H_2O, 0.025 g L^{-1} $MnSO_4 \times H_2O$, 0.4 g L^{-1} $CuSO_4 \times 5$ H_2O, 0.045 g L^{-1} $CoCl_2 \times 6$ H_2O, 2.2 g L^{-1} $CaCl_2 \times 2$ H_2O, and 50 g L^{-1} $MgSO_4 \times 7$ H_2O. All chemicals were purchased from Carl Roth GmbH + Co. KG, Karlsruhe, Germany.

2.3 Reactor Setup

The reactor housing, with an inner diameter of 3 cm and a height of 20 cm, was fabricated of transparent polycarbonate (Makrolon, Covestro Deutschland AG, Leverkusen). Gas was sparged via a sealed sinter plate at the bottom of the reactor. The porous area of the plate had a cross-sectional diameter of 30 mm and a pore size range of 10–16 µm. Temperature was measured by a sheath thermocouple type-K (Therma Thermofühler GmbH, Lindlar, Germany) and controlled by circulation of heated water (A 106, Lauda Dr. R. Wobser GmbH & Co. KG, Lauda-Königshofen, Germany) through a heating pipe located in the reactor. All experiments were performed with a liquid volume of 60 mL (see Fig. 1).

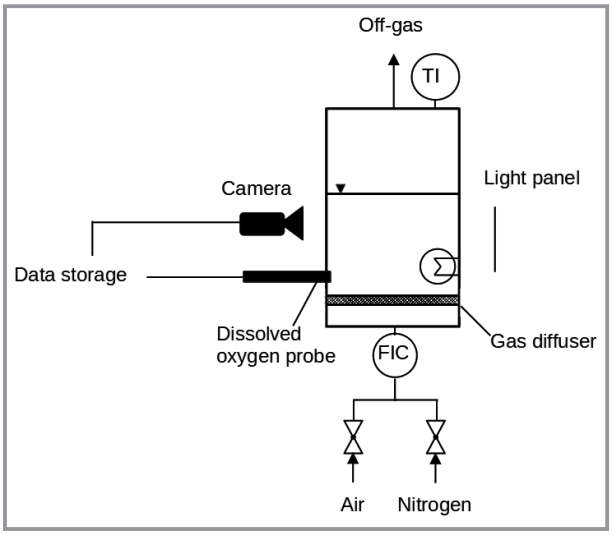

Figure 1. Experimental setup for gas holdup, k_La and bubble size measurement.

2.4 Bubble Size Distribution Measurement

In order to measure the bubble size distribution (BSD), a digital imaging (DI) procedure was used. As the DI method is limited to the simultaneous analysis of a low number of bubbles only, the analyzed liquid and aerated volume was artificially reduced. To be precise, by shortening the diameter of the sinter plate from 30 to 7.5 mm, it was feasible to decrease the gas volume flow to 1/16 while maintaining the same superficial gas velocity as applied for k_La and gas holdup measurements. To avoid distortion effects in the cylindrical reactor shape, the study was carried out in a rectangular reactor constructed for this purpose. In addition to constant u_G values for different sparger diameters, the same pore Reynolds numbers (Re_p) were maintained. Re_p can be calculated by using u_G, mean pore diameter (d_p), taken from the sparger data sheet and kinematic viscosity of air (ν_G).

$$Re_p = \frac{u_G d_p}{\nu_G} \tag{1}$$

For both reactors the Re_p was between $1.8 \cdot 10^{-3}$ and $4.5 \cdot 10^{-3}$ for the u_G range considered in this study. The temperature was kept at 37 °C during the measurement.

 © 2023 The Authors. Chemie Ingenieur Technik published by Wiley-VCH GmbH

Bubbles were detected in the flat chamber with dimensions of (L, W, H) of (250 mm, 30 mm, 120 mm). The superficial gas velocity u_G at the inlet, calculated by division of the gas volume flow by the cross-sectional area of the sparger plate, varied between 0.12 and 0.59 cm s^{-1}. The reactor was placed between a camera and a homogeneous (LED) panel and the bubbles were recorded at a height of 40 mm above the sinter plate. Using Matlab an individual algorithm was programmed for automated evaluation of the pictures. For each BSD, at least 110 pictures were analyzed, comprising 2500–20 000 bubbles. An exposure time of 1/8000 s was chosen to sharply emphasize the contours of the bubbles. A constant and narrow focal plane was chosen such that out-of-focus bubbles could be sorted out during post processing. The uncompressed raw images were converted into a binary pixel matrix using the Sobel operator [14], to attribute individual pixels to bubbles. In Fig. 2a, an unmodified raw photo is shown, which is then converted into a binary photo seen in Fig. 2b.

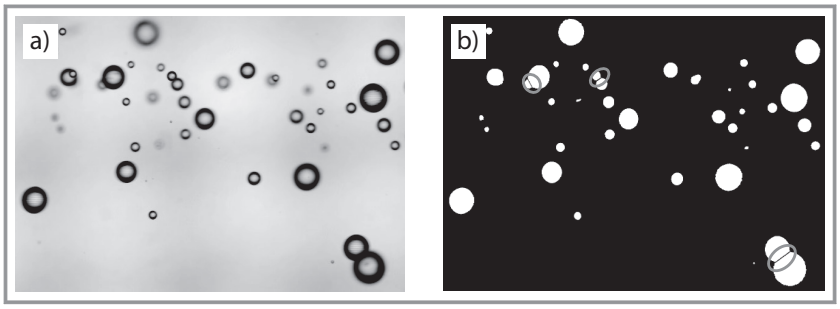

Figure 2. Mechanism of the automated throughput DI algorithm. a) Unmodified raw picture, b) binary photo with automated separated bubbles.

Using a photographed reference length, the conversion factor between pixel number and millimeters was determined for each image series. Single or double superimposed bubbles were automatically separated by applying the convex hull criterion [14], as highlighted in Fig. 2b. Larger cluster of bubbles were detected and sorted out on the basis of size and shape. In addition to the size distribution, the characteristic Sauter diameter d_{32} was determined. As indicated in Eq. (2), d_{32} indicates the bubble diameter resulting from the conversion of the real bubble size distribution into bubbles of equal size maintaining the ratio of volume to surface area.

$$d_{32} = \frac{\sum_{i=1}^{\infty} d_i^3}{\sum_{i=1}^{\infty} d_i^2} \tag{2}$$

2.5 Gas Holdup Measurement

The gas content in deionized water, medium and PBS buffer was measured using a DI method. The u_G varied between 0.12 and 0.59 cm s^{-1} and the reactor wall was replaced by a transparent tube of the same diameter and positioned between the camera and a light source. Pictures bevor and after the rising of the fluid level were taken and automatically evaluated by an imaging process script using Matlab.

By combining the grayscale and Sobel operator criteria [14], the liquid height could be identified, as seen in Fig. 3. For each setting, a mean value analyzing 25 images was calculated. The conversion into millimeters was done on the basis of a photographed reference length. Then, the gas holdup was calculated (see Eq. (3)):

$$\varepsilon = \frac{\Delta H_{aerated}}{\Delta H_{aerated} + H_0} \tag{3}$$

2.6 Mass Transfer Calculations

With the information of gas holdup and d_{32} it is possible to compute the specific surface area:

$$a = \frac{6\varepsilon}{d_{32}(1-\varepsilon)} \tag{4}$$

Having determined both the k_La and a, k_L can be further identified as follows:

$$k_L = \frac{k_L a}{a} \tag{5}$$

3 Results and Discussion: Influence of Superficial Gas Velocity

3.1 Sauter Mean Diameter

Fig. 4 depicts d_{32} for different superficial gas velocities comparing bubble diameters of water, PBS buffer, minimal

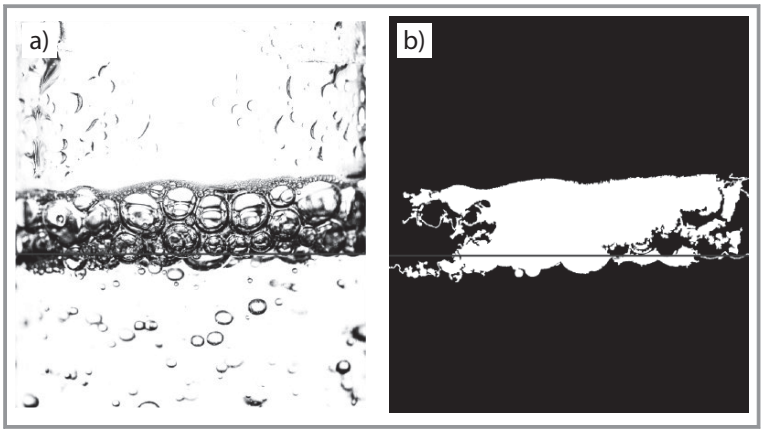

Figure 3. Mechanism of the automated gas holdup measurement. a) Unmodified raw picture, b) binary photo with automated liquid and foam separation.

 © 2023 The Authors. Chemie Ingenieur Technik published by Wiley-VCH GmbH

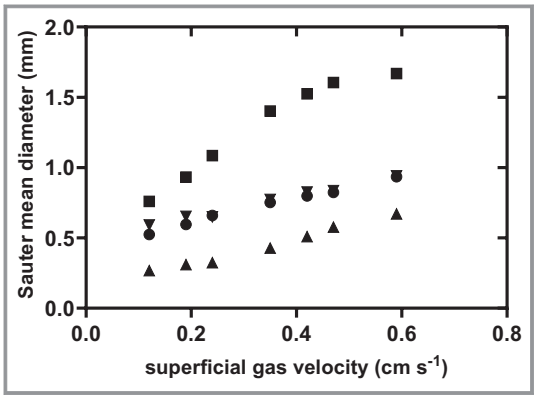

Figure 4. Sauter mean diameter for deionized water (□), 1 × PBS solution (●), minimal medium (▲) and minimal medium + AF (▼) at different superficial gas velocities.

medium, and minimal medium with antifoam (AF). In minimal medium the bubbles are the smallest irrespective of u_G. Starting from u_G of 0.11 cm s^{-1} and d_{32} of 0.27 mm, values are increasing to 0.67 mm at u_G = 0.59 cm s^{-1}. Largest bubbles are found in pure water where d_{32} increases from 0.76 to 1.67 mm with rising u_G from 0.12 to 0.59 cm s^{-1}. In general, it is well known that medium components strongly affect bubble size, as it is visible for the three-fold range of bubble sizes depicted in Fig. 4. This is why the use of minimal medium leads to the smallest bubble sizes. On contrary, the addition of AF leads to larger bubbles, similar to the use of phosphate buffer solution (PBS). For both, minimal medium and minimal medium with AF, Sauter diameters vary between 0.59 and 0.94 mm. Given that electrolytes are known to prevent coalescence finally yielding the smallest Sauter diameter for the minimal medium [16], it may be concluded that the phosphate addition in PBS did not cause equal ion strength as in the minimal medium. Apparently, coalescence suppression is less than in minimal medium. Beside of electrolytes, the bubble size is influenced by glucose in the medium. Organic substances inhibit the coalescence resulting in smaller bubbles. Recently, the latter has been demonstrated by [17] investigating the impact of ethanol in gas fermentation. Regarding the impact of AF, multiple mechanisms are considered in literature [18–21]. According to [20], AF may lower the surface tension, which destabilizes large bubbles. On contrary, coalescence is enhanced yielding larger d_{32}. Which effect dominates is hardly predictable. It was shown in [21] that the addition of octamethyltetrasiloxane stabilized small bubbles whereas polyethylene glycol increased the Sauter diameter by trend. As the antifoam (Struktol® J 647) consists of polyglycol ethers the observations of [21] is confirmed (see Fig. 4).

3.2 Bubble Size Distribution and Sauter Diameter

To investigate how the superficial gas velocity may affect the bubble size distribution, different aeration rates were studied for water. Fig. 5 plots a selection of three resulting BSDs in a histogram. Regarding the smallest superficial gas velocity of 0.12 cm s^{-1} the majority of the bubbles was found between 0.2 and 0.4 mm. With increasing u_G the distribution shifted to larger bubble sizes with less bubbles in the smallest size bin. Bubbles larger than 1.2 mm only occur with a frequency of < 1 %. At u_G of 0.59 cm s^{-1} the distribution converges to uniform in the range from 0.2 to 1.1 mm. Single bubbles occur with maximum size of 2.8 mm. The histogram outlines that the Sauter diameter increases with rising u_G because the number of small bubbles decreases. In parallel, the BSD variance grows too, as d_{32} converges to constant values.

Further BSD studies were conducted investigating BSD and Sauter diameters for u_G ranging from 1.13 to 2.64 cm s^{-1}. As depicted in Fig. 6, the d_{32} trend may be divided into a linear rise between u_G of 1.13 cm s^{-1} to 2.04 cm s^{-1} with a slope

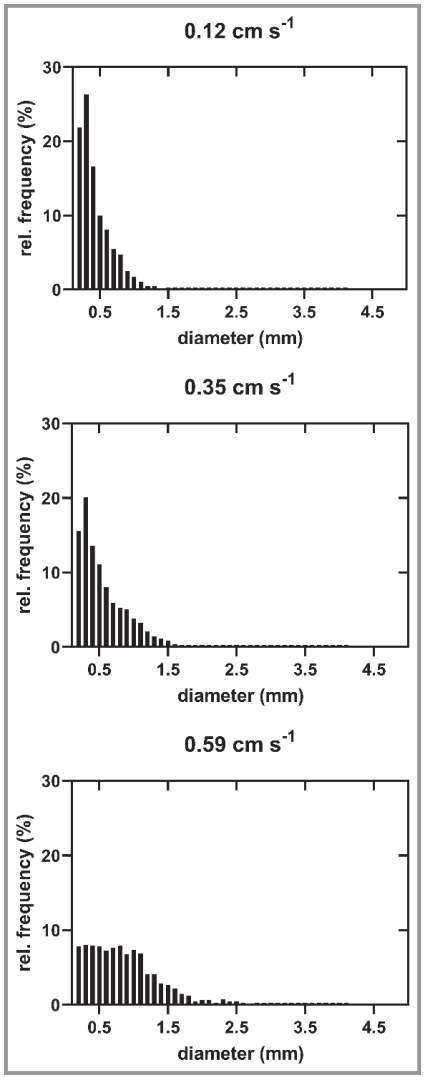

Figure 5. Histogram of relative frequency of the Sauter mean diameter for 3 different superficial gas volume flows.

 © 2023 The Authors. Chemie Ingenieur Technik published by Wiley-VCH GmbH

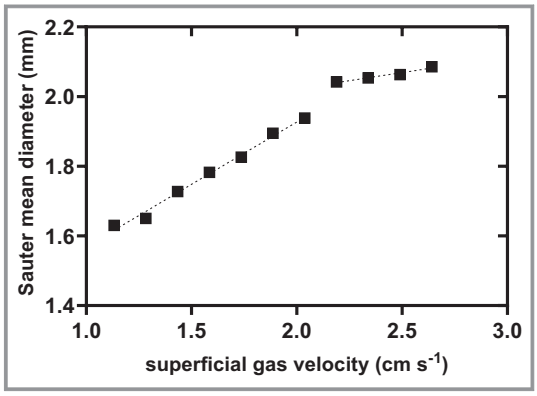

Figure 6. Sauter mean diameter at different superficial gas velocities in water.

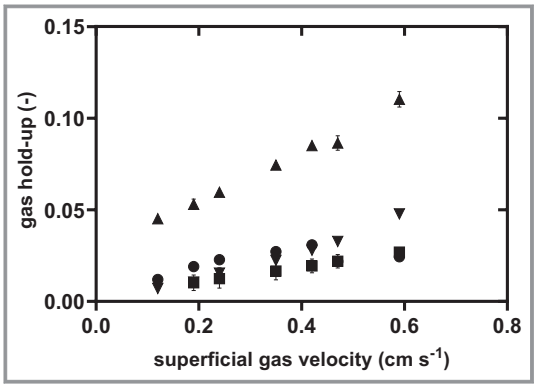

Figure 7. Gas holdup for deionized water (□), 1 × PBS solution (●), minimal medium (▲) and minimal medium + AF (▼) at different superficial gas velocities.

of 0.36, followed by an aeration scenario leading to rather constant d_{32} of 2.08 mm.

Multiple studies analyzing the Sauter diameter in bubble columns [6–8, 18, 22, 23] observed increasing d_{32} with elevated u_G. The study of [7] predicted bubble sizes between 0.75 to 1.6 mm were using plates with pores of 16 and 40 µm whereas [8] measured d_{32} between 0.31 and 1.8 mm. Bhavaraju et al [23] outlined that a positive correlation between bubble size and superficial gas velocity is only observable for a particular aeration regime when surface tension becomes negligible and bubble sizes are determined by the balance between buoyancy, inertial, and viscous forces. Then, the bubbles are filled proportionally to the contact time at the porous plates. Rising aeration reaches a maximum of bubble size that cannot be exceeded [23]. This effect is shown in Fig. 6 for $u_G > 2.04\,\mathrm{cm\,s^{-1}}$. The empirical correlations of [23] and [18] cannot reflect exactly the trend of Fig. 6, maybe because additional effects such as proper wetting of the sparger surface [18] and increasing breakthrough pressure for small pore diameters [6] need to be considered, too.

3.3 Gas Holdup

In Fig. 7 the experimentally determined gas holdup ε for water, medium, medium with AF and PBS buffer is shown. For all liquids, ε increases proportionally with u_G. The largest rise of about 4-fold is observed for the AF medium showing the smallest gas holdup at $0.12\,\mathrm{cm\,s^{-1}}$AF. Similar trends are found for PBS buffer and water reaching ε of 0.024 and 0.026 at the highest air flow rate of $0.59\,\mathrm{cm\,s^{-1}}$, respectively. The highest gas holdup was measured for minimal medium without AF outcompeting the other media by approximately factor 3.

The gas holdup is almost exclusively determined by the bubble diameter and the air flow rate. Larger bubbles represent large air volume but have a shorter residence time due to a faster ascent rate. The relationship between bubble size and velocity is mainly given by the drag force. One of the most common drag force models by [24] shows a nonlinear relationship between bubble diameter and rising velocity. This is reflected by the maximum gas holdup at $0.43\,\mathrm{cm\,s^{-1}}$ for PBS buffer, which indicates that the increase of d_{32} does not necessarily lead to faster bubbles. Considering Fig. 4 it is well observable that the largest gas holdup in Fig. 7 found for minimal medium corresponds to the smallest bubble size. By analogy, this holds also true for the largest bubbles leading to the lowest gas holdup in water. In the study of [7] the gas holdup of a small-scale bubble column was measured between 0.02 and 0.1 under fermentation conditions. This shows that the range considered here reflects relevant cultivation conditions. The effect that AF addition lowers gas holdups was also confirmed in other studies [18, 21].

3.4 Mass Transfer

To study how k_La correlates with the superficial gas velocity, a series of aeration tests were performed using the same set of media and covering the same aeration rates as installed in the studies (see Fig. 8). Mass transfer coefficients ranging from $0.025\,\mathrm{s^{-1}}$ to $0.2\,\mathrm{s^{-1}}$ were found, which is in agreement with similar studies [6, 7]. k_La values correlate linearly with u_G (R^2 = 0.99/0.97/0.97/0.97 for water/PBS/MM MM + AF), a phenomenon that has been observed in small-scale bubble column reactors previously [6]. The k_La divides two groups with values for deionized water being the smallest whereas the rest cannot be distinguished statistically.

As outlined in [25] the increase of oxygen transfer in aqueous solutions with rising electrolyte concentration up to 0.1 M. Further electrolyte increase did not improve k_La. For both, 1 x PBS and the minimal media solutions, this upper limit of electrolyte content is exceeded which may explain the similar oxygen transfer performance.

Studies of [7] did not find any impact of low AF concentrations (0.02 vol %) on k_La in minimal medium. Indeed, Fig. 8 anticipates the same conclusion but diving into the individual impacts of a and k_L reveals remarkable details:

 © 2023 The Authors. Chemie Ingenieur Technik published by Wiley-VCH GmbH

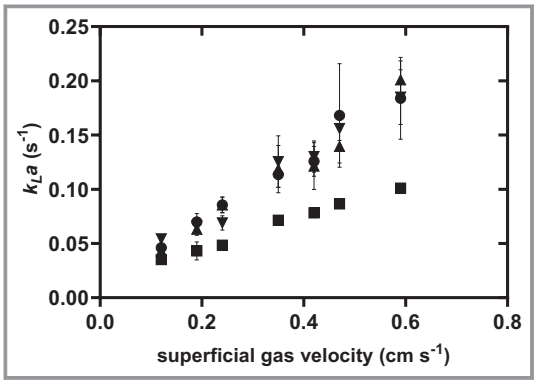

Figure 8. Volume specific oxygen transfer coefficient for deionized water (□), 1 × PBS solution (●), minimal medium (▲) and minimal medium + AF (▼) at different superficial gas velocities.

Namely, that any improvement in k_La is mainly due to rising k_L with aeration while a remains stable.

The explanation is as follows: The volume specific surface area a is calculated from the measured gas holdup and d_{32} (Eq. (4)). Next, k_L is derived from known a and k_La (Eq. (5)). Because of the largest bubble sizes, a is smallest for deionized water and largest for minimal media exceeding deionized water 10-fold. Interestingly, the specific surface area a is stable over the observed range for most of the investigated liquids (see Fig. 10). Only AF supplemented minimal media shows a linear increase (R^2 = 0.92) with aeration. Hence, all other media – except AF – increase in bubble diameter with u_G (Figs. 4–6) with equally rising ε (Fig. 7).

For k_L, large differences occur between the observed liquids as can be seen in Fig. 9. It is found that the presence of solutes seems to influence k_L on multiple ways, which is in line with findings of [12]. This might be explained by additional mass transfer resistance created by the ionic film at the boundary layer [10] and reduced diffusion coefficients in the presence of solutes [15]. Furthermore, reducing bubble size also decreases the bubble rising velocity, which lowers the interfacial slip velocity and hence reduces k_L [26]. As dissolved ions [10] and glucose [27] increase the viscosity of a solution, the combined effect of physicochemical liquid properties and bubble size is strongest for the minimal media solution and results in the lowest k_L values of $1 \cdot 10^{-4}$ m s^{-1}.

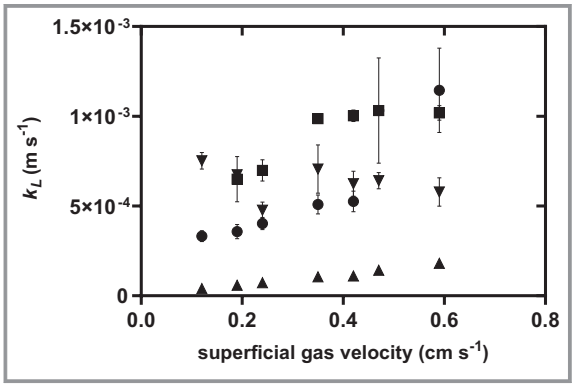

Figure 9. Mass transfer coefficient k_L for deionized water (□), 1 × PBS solution (●), minimal media (▲) and minimal media + AF (▼) at different superficial gas velocities.

Our findings do not support the theory of constant mass transfer coefficients for bubbles smaller than 1.5 mm as suggested by [28]. One explanation could be that we gathered more data points in this particular operating regime whereas [28] only evaluated bubble sizes > 1 mm. It is noted that the estimation of k_L is prone to error as it contains uncertainties of k_La, ε and bubble size measurements, which explains the large errors for some data points. Though, for deionized water, PBS and minimal media an increase in k_L with u_G is found. For minimal media, water and PBS it is found, that an increase in u_G and resulting larger bubbles, do not lead to higher specific surface area and thus do not influence the k_La. The increase in k_La with u_G is the result of enhanced mass transfer coefficient. These findings suggest that the volume specific surface area a is the rate limiting step in optimizing oxygen transfer.

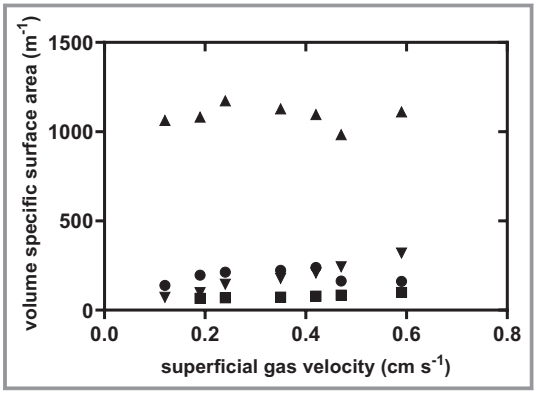

Figure 10. Volume specific surface area a for deionized water (□), 1 × PBS solution (●), minimal media (▲) and minimal media + AF (▼) at different superficial gas velocities. Error bars are smaller than the symbol size.

4 Conclusion and Outlook

In the current study, bubble size distributions, gas holdup, and k_La values were measured for various liquids applying relevant fermentation conditions for bubble columns. The separation of the k_La value into a and k_L revealed that the influence of the Sauter diameter and the gas holdup on a compensate each other whereas k_L increases with rising superficial gas velocity. The latter mirrors the linear relationship between the Sauter diameter and the superficial gas velocity that converges to a constant d_{32} for high superficial velocities. In turn, the observation reveals that further k_La improvements are tightly linked with liquid properties to lower bubble sizes by altering surface tension.

Consequently, a turns out as the limiting factor for mass transfer in bubble columns, which puts further emphasis on future media designs. Furthermore, the findings may

 © 2023 The Authors. Chemie Ingenieur Technik published by Wiley-VCH GmbH

provide a sound basis for designing large-scale bubble columns via sophisticated computational fluid dynamic approaches.

We would like to thank Andreas Freund and Leon Borck for their support in conducting the experiments. Open access funding enabled and organized by Projekt DEAL.

Symbols used

a	[m^{-1}]	volume specific interfacial area
d_p	[µm]	pore diameter
d_{32}	[mm]	Sauter mean diameter
H	[mm]	reactor height
k_L	[$m\,s^{-1}$]	liquid side mass transfer coefficient
k_La	[s^{-1}]	integral volumetric mass transfer coefficient
R^2	[–]	coefficient of determination
Re_p	[–]	pore Reynolds number
u_G	[$cm\,s^{-1}$]	superficial gas velocity
ν_G	[m^2s^{-1}]	kinematic viscosity of gas phase
ε	[–]	gas holdup

Abbreviations

AF	Antifoam
BSD	Bubble size distribution
DI	Digital imaging
PBS	Phosphate buffer solution

References

[1] S. Kheradmandnia, S. Hashemi-Najafabadi, S. A. Shojaosadati, S. M. Mousavi, K. Malek Khosravi, *J. Chem. Technol. Biotechnol.* **2015**, *90 (6)*, 1051–1061. DOI: https://doi.org/10.1002/jctb.4408

[2] J. I. Betts, F. Baganz, *Microb. Cell Fact.* **2006**, *5 (1)*, 21. DOI: https://doi.org/10.1186/1475-2859-5-21

[3] S. J. Wewetzer, M. Kunze, T. Ladner, B. Luchterhand, S. Roth, N. Rahmen, R. Kloß, A. Costa, E. Silva, L. Regestein, J. Büchs, *J. Biol. Eng.* **2015**, *9*, 9. DOI: https://doi.org/10.1186/s13036-015-0005-0

[4] P. R. Patnaik, *Int. J. BIOautom.* **2015**, *19 (S1)*, S1–S42.

[5] B. Moshtari, E. G. Babakhani, J. S. Moghaddas, *Pet. Coal* **2009**, *51 (1)*, 27–32.

[6] S. D. Doig, A. Diep, F. Baganz, *Biochem. Eng. J.* **2005**, *23 (2)*, 97–105. DOI: https://doi.org/10.1016/j.bej.2004.10.014

[7] D. Weuster-Botz, J. Altenbach-Rehm, A. Hawrylenko, *Bioprocess Biosyst. Eng.* **2001**, *24 (1)*, 3–11. DOI: https://doi.org/10.1007/s004490100222

[8] S. Khanchezar, S. Hashemi-Najafabadi, S. A. Shojaosadati, V. Babaeipour, *Bioprocess Biosyst. Eng.* **2019**, *42 (2)*, 257–266. DOI: https://doi.org/10.1007/s00449-018-2030-0

[9] G. Besagni, F. Inzoli, T. Ziegenhein, *ChemEngineering* **2018**, *2 (2)*, 13. DOI: https://doi.org/10.3390/chemengineering2020013

[10] S. A. Baz-Rodríguez, J. E. Botello-Alvarez, A. Estrada-Baltazar, L. E. Vilchiz-Bravo, J. A. Padilla-Medina, R. Miranda-López, *Chem. Eng. Res. Des.* **2014**, *92 (11)*, 2352–2360. DOI: https://doi.org/10.1016/j.cherd.2014.02.023

[11] N. Kantarci, F. Borak, K. O. Ulgen, *Process Biochem.* **2005**, *40 (7)*, 2263–2283. DOI: https://doi.org/10.1016/j.procbio.2004.10.004

[12] A. Ferreira, P. Cardoso, J. A. Teixeira, F. Rocha, *Chem. Eng. Sci.* **2013**, *100*, 145–152. DOI: https://doi.org/10.1016/j.ces.2013.02.020

[13] M. Löffler, J. D. Simen, G. Jäger, K. Schäferhoff, A. Freund, R. Takors, *Metab. Eng.* **2016**, *38*, 73–85. DOI: https://doi.org/10.1016/j.ymben.2016.06.008

[14] R. C. Gonzalez, *Digital image processing*, 3rd ed., Addison-Wesley Publishing Company, Pearson Prentice Hall, Reading, MA, **2007**.

[15] M. Jamnongwong, K. Loubiere, N. Dietrich, G. Hébrard, *Chem. Eng. J.* **2010**, *165 (3)*, 758–768. DOI: https://doi.org/10.1016/j.cej.2010.09.040

[16] V. Machon, A. W. Pacek, A. W. Nienow, *Chem. Eng. Res. Des.* **1997**, *75 (3)*, 339–348. DOI: https://doi.org/10.1205/026387697523651

[17] L. Puiman, M. P. Elisiário, L. M. Crasborn, L. E. Wagenaar, A. J. Straathof, C. Haringa, *Biochem. Eng. J.* **2022**, *185*, 108505. DOI: https://doi.org/10.1016/j.bej.2022.108505

[18] K. Koide, S. Yamazoe, S. Harada, *J. Chem. Eng. Jpn.* **1985**, *18 (4)*, 287–292. DOI: https://doi.org/10.1252/jcej.18.287

[19] D. D. McClure, M. Lamy, L. Black, J. M. Kavanagh, G. W. Barton, *Chem. Eng. Sci.* **2017**, *160*, 269–274. DOI: https://doi.org/10.1016/j.ces.2016.11.033

[20] A. Morão, C. I. Maia, M. M. R. Fonseca, J. M. T. Vasconcelos, S. S. Alves, *Bioprocess Eng.* **1999**, *20 (2)*, 165. DOI: https://doi.org/10.1007/s004490050576

[21] D. D. McClure, J. Deligny, J. M. Kavanagh, D. F. Fletcher, G. W. Barton, *Chem. Eng. Technol.* **2014**, *37 (4)*, 652–658. DOI: https://doi.org/10.1002/ceat.201300711

[22] S. D. Doig, K. Ortiz-Ochoa, J. M. Ward, F. Baganz, *Biotechnol. Prog.* **2005**, *21 (4)*, 1175–1182. DOI: https://doi.org/10.1021/bp050064j

[23] S. M. Bhavaraju, T. W. F. Russell, H. W. Blanch, *AIChE J.* **1978**, *24 (3)*, 454–466. DOI: https://doi.org/10.1002/aic.690240310

[24] A. Tomijama, I. Kataoka, I. Zun, T. Sakaguchi, *JSME Int. J., Ser. B* **1998**, *41 (2)*, 472–479. DOI: https://doi.org/10.1299/jsmeb.41.472

[25] A. M. Al Taweel, A. O. Idhbeaa, A. Ghanem, *Chem. Eng. Sci.* **2013**, *100*, 474–485. DOI: https://doi.org/10.1016/j.ces.2013.06.013

[26] Y. T. Shah, B. G. Kelkar, S. P. Godbole, W.-D. Deckwer, *AIChE J.* **1982**, *28 (3)*, 353–379. DOI: https://doi.org/10.1002/aic.690280302

[27] V. Telis, J. Telis-Romero, H. B. Mazzotti, A. L. Gabas, *Int. J. Food Prop.* **2007**, *10 (1)*, 185–195. DOI: https://doi.org/10.1080/10942910600673636

[28] R. Sardeing, P. Painmanakul, G. Hébrard, *Chem. Eng. Sci.* **2006**, *61 (19)*, 6249–6260. DOI: https://doi.org/10.1016/j.ces.2006.05.051

 © 2023 The Authors. Chemie Ingenieur Technik published by Wiley-VCH GmbH